

Lagrangian Manifestation of Anomalies in Active Turbulence

Rahul K. Singh,^{*} Siddhartha Mukherjee,[†] and Samriddhi Sankar Ray[‡]

International Centre for Theoretical Sciences, Tata Institute of Fundamental Research, Bangalore 560089, India

We show that Lagrangian measurements in active turbulence bear imprints of *turbulent* and anomalous *streaky* hydrodynamics leading to a self-selection of persistent trajectories—*Lévy walks*—over diffusive ones. This emergent dynamical heterogeneity results in a super-diffusive *first passage* distribution which could lead to biologically advantageous motility. We then go beyond single-particle statistics to show that for the pair-dispersion problem as well, active flows are at odds with inertial turbulence. Our study, we believe, will readily inform experiments in establishing the extent of universality of anomalous behaviour across a variety of active flows.

INTRODUCTION

Flowing active matter, such as dense suspensions of bacteria, has emerged as one of the most intriguing class of problems in complex, driven-dissipative systems which sits at the intersection of non-equilibrium statistical physics, biophysics, soft-matter and of course fluid dynamics [1–4]. What makes such low Reynolds number systems particularly fascinating is the emergence of rich and complex collective patterns at scales much larger than, but driven by, relatively simpler individual dynamics [1, 2, 5, 6] as well as its ubiquity across systems as diverse as bacterial colonies [7, 8], suspensions of microtubules and molecular motors [9–11], or schools of fish [12] and bird flocks [1, 13, 14]. In dense active systems, typically those involving microscopic entities, the interactions between individual agents lead to unorganized, often vortical, dynamics with self-similar distribution of energy across several length scales. This last aspect, namely the *appearance* of the flow field and the power-laws which emerge in measurements of the kinetic energy across Fourier modes [4, 7, 15, 16], lead to such states being called *active turbulence* in analogy with similar traits of high Reynolds number inertial turbulence [4].

However, there are important distinctions between inertial and active turbulence. The most striking of these being that unlike high Reynolds number flows, experiments suggest non-universal signatures of Lévy walks and anomalous diffusion in measurements of mean-square-displacements (MSDs) in active suspensions [17–20]. These observations were substantiated in a recent theoretical work [21] which showed not only the robustness of the anomalous diffusion and its coincidence with the emergence of novel, *streaky* structures in the flow for optimal activity, but also why in earlier theoretical studies [22] such a scaling regime remained masked.

The fact that trajectories of tracers in such systems show Lévy statistics is consistent with other examples from the natural world where *active agents* Lévy walk or fly [23–27]. Nevertheless, this throws up interesting questions regarding the nature of trajectories and hence, fundamental issues of Lagrangian turbulence in such dense bacterial suspensions. In particular, a consequence of this could well be that while for low activities, trajectories are nearly always meandering (hence diffusive), at higher activities, there is a balance between those which follow Lévy statistics and those which do not. In fact, even for a given tracer it is conceivable that depending on the flow it experiences, its trajectory could either be persistent or random.

We address some of these issues relevant to dense (and dry) bacterial suspensions, by taking a continuum, numerical approach to the problem. The generalized hydrodynamic model (see, also, Refs. [7, 28] for a detailed description), which is essentially a modified version of the Navier-Stokes equation employing terms that lead to pattern formation (similar to Swift-Hohenberg theory [29]) and flocking behaviour (Toner-Tu theory [30, 31]), is used to simulate the evolution of the coarse-grained velocity field \mathbf{u} of bacterial suspensions, and is given as:

$$\partial_t \mathbf{u} + \lambda \mathbf{u} \cdot \nabla \mathbf{u} = -\nabla p - \Gamma_0 \nabla^2 \mathbf{u} - \Gamma_2 \nabla^4 \mathbf{u} - (\alpha + \beta |\mathbf{u}|^2) \mathbf{u} \quad (1)$$

where \mathbf{u} satisfies the incompressibility constraint $\nabla \cdot \mathbf{u} = 0$. The parameter $\lambda > 1 (< 1)$ corresponds to pusher (puller)-type bacteria while the higher order derivatives along with the non-linear self-advective term drive the formation of chaotic flow patterns when $\Gamma_0, \Gamma_2 > 0$. A key difference is that the usual diffusion term of the Navier-Stokes equation appears with the opposite sign, and acts towards inducing a turbulence instability in the bacterial system, while the

^{*} rksphys@gmail.com

[†] siddhartha.m@icts.res.in

[‡] samriddhisankarray@gmail.com

additional bi-Laplacian term aids dissipation. The last term is a Toner-Tu drive [30, 31], which is effectively a quartic Landau-potential for the velocity, with the activity α taking both positive (friction) and negative (active injection) values, while β is strictly positive for stability and causes most of the momentum dissipation. For driven active systems ($\alpha < 0$), this term leads to global polar ordering with a velocity $v_0 = \sqrt{|\alpha|/\beta}$.

In our simulations, we solve Eq. (1) by using a de-aliased, pseudo-spectral algorithm on square, periodic domains of lengths $L \in \{20, 40, 80\}$ which are discretized by using $N^2 \in \{1024^2, 4096^2\}$ collocation points. The simulations are performed for 5×10^5 iterations with time-steps $\delta t = 0.001$ and, in some cases, $\delta t = 0.0002$ for higher temporal resolution (note that a simulation time of ~ 30 is ~ 1 minute of real time [7]). The other parameters of the model are taken to be consistent with earlier studies [21, 32–34], and these were carefully chosen to reproduce the physically observed flow patterns and Eulerian statistics [7]. Here, $\Gamma_0 = 0.045$, which corresponds to $-53 \mu\text{m}^2/\text{s}$, $\Gamma_2 = \Gamma_0^3$ and $\lambda = 3.5$ [7]. The swarming speed of *Bacillus subtilis*, which is linked to the activity, can vary over a wide range of $25\text{--}100 \mu\text{m}/\text{s}$, depending on the oxygen concentration of the system and the boundary conditions [7, 20, 35, 36]. These velocities in the experiment are associated with the typical velocities which arise in the hydrodynamic description: $v_\Gamma = \sqrt{|\Gamma_0|^3/\Gamma_2}$ or $v_0 = \sqrt{|\alpha|/\beta}$. An empirical comparison between simulations and experiments (see [7], Supporting Information) suggested that $\alpha = -1$ and $\beta = 0.5$ (simulation units) corresponded to $-0.5/\text{s}$ and $4 \times 10^{-4} \text{s}/\mu\text{m}^2$ (physical experimental units), respectively. These physical units correspond to a velocity scale $\sim 35 \mu\text{m}/\text{s}$, with the corresponding simulation velocity scale $v_0 = \sqrt{|\alpha|/\beta} = \sqrt{2}$. However, as was shown in a recent theoretical study [21], phenomena like anomalous diffusion and Lévy walks, that were recently observed in experiments [20], *only* become robust at sufficiently high activity levels in simulations (around $\alpha = -6$). Therefore, while keeping $\beta = 0.5$ fixed, we vary the activity over a wide range $-6 \leq \alpha \leq -1$. We note that the highest value of $\alpha = -6$ yields $v_0 \approx 2.4\sqrt{2}$ (simulation units) or $v_0 \approx 72 \mu\text{m}/\text{s}$ (choosing, for convenience, the average velocity in the range $25 \mu\text{m}/\text{s} - 35 \mu\text{m}/\text{s}$ reported by [7] as reference), which is well within the physically viable range of bacterial velocities [7, 36]. We caution the reader that this mapping of parameters should be seen as a rough guide, since the calibration of coefficients between theory and experiments is largely empirical. Lastly, the flow is seeded with 10^5 randomly distributed tracers which evolve as $d\mathbf{x}/dt = \mathbf{u}(\mathbf{x}(t))$, with $\mathbf{x}(t)$ being the tracer location at time t , after a spinup time of 2×10^4 iterations (when the flow reaches a statistically steady state). We use a fourth-order Runge-Kutta scheme, along with a bilinear interpolation scheme to obtain the fluid velocity at the particle positions $\mathbf{u}(\mathbf{x}(t))$, to evolve the tracers with statistics being stored every 100 iterations.

In Fig. 1(a) we show representative trajectories from our simulations with increasing levels of activity. While for suspensions with low activity ($\alpha = -1$), the particle motion is predominantly diffusive with large, *knotted* regions of *random-walk*, the more active fields ($\alpha = -4$) give rise to trajectories which have a persistent motion showing characteristic signatures of Lévy walks; a precise definition of the activity parameter α is given below. However, these Lévy-like, persistent trajectories are only one part of the story. Careful measurements in these simulations indicate that even at higher activity ($\alpha = -6$) it is easy to find in an ensemble trajectories that are persistent (Fig. 1(b)) and those that remain predominantly diffusive (Fig. 1(c)); see also <https://youtu.be/CPJ3Z1XBf-k>. (We note that the trajectories were artificially moved to a common center for visualization; in simulations, their origins are distributed randomly at different points in the flow.)

This leads us to critically examine the nature of trajectories in such highly active systems and establish connections between anomalies of the emergent coarse-grained velocity field and its effect on the resultant Lagrangian statistics. As a result we uncover a remarkable dynamical heterogeneity in trajectories, implicit in Fig. 1, and its critical role in assisting the swarm for efficient foraging through first-passage statistics. We also show, in a way which is easily amenable to experiments, that such persistent motion are facilitated by the novel, emergent structures in the bacterial field—*streaks*—which have no known counterparts in inertial, high Reynolds number turbulence. We conclude by going beyond single-particle statistics and investigating the pair-dispersion problem in active turbulence.

Trajectories, especially for high activity, often comprise of long walking-segments of varying step-lengths, interspersed with turning points as seen in Figs. 1(a) and 1(b). Identifying the “turns” [20, 21] is then crucial to segment trajectories into their constituent step-lengths (and waiting-times) for the analysis that follows. This is done by first calculating a turning angle θ at each point along the trajectory at time intervals Δt as $\cos(\theta(t)) = \frac{\Delta\mathbf{r}(t) \cdot \Delta\mathbf{r}(t+\Delta t)}{|\Delta\mathbf{r}(t)| |\Delta\mathbf{r}(t+\Delta t)|}$, where $\Delta\mathbf{r}(t) = \mathbf{r}(t) - \mathbf{r}(t - \Delta t)$; our results are insensitive for a wide range of Δt . Walking-segments and turns can be identified using a threshold $\theta(t) > \theta_c$, which in turn gives the step-lengths d and waiting-times τ of the segments between successive turns. We choose $\theta_c = 30^\circ$ for this study [21] and have checked that our results remain unchanged for $25^\circ \leq \theta_c \leq 45^\circ$.

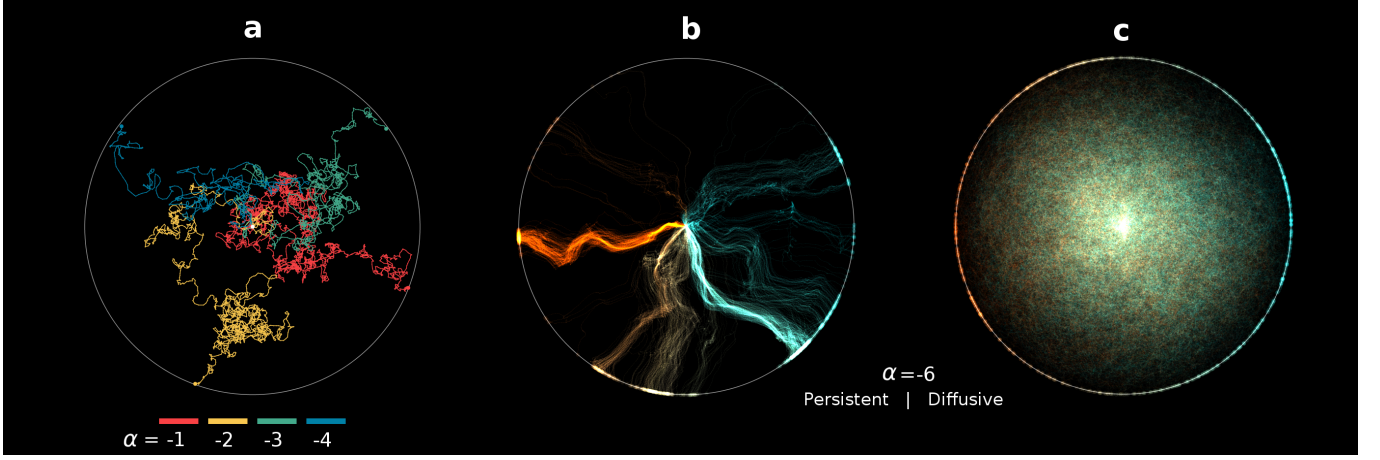


FIG. 1. Representative trajectories for (a) suspensions with different degrees of activity α (see Eq. (1)) as well as for highly active suspensions showing the (b) fastest 1% tracers, that are persistent and anisotropic and (c) slowest 1% tracers that are diffusive and isotropic. Different trajectories are translated to a common origin for clarity and the color variation is a function of the angle at which they reach the bounding circle while the brightness is proportional to the density of trajectories; see also <https://youtu.be/CPJ3Z1XBf-k>. (These images, and Fig. 3, were generated with Processing [37, 38]).

FAST AND SLOW TRAJECTORIES AND THE ROLE OF EMERGENT FLOW STRUCTURES

Do tracers in highly active suspensions ($\alpha = -6$) show a bias in the way they sample the relatively weaker and stronger vorticity $\omega = \nabla \times \mathbf{u}$ regions of the flow (Fig. 2(a))? The probability distribution function (pdf) of the vorticity field normalised by $\omega' = \sqrt{\langle \omega^2 \rangle}$, where $\langle \cdot \rangle$ denotes spatial averaging, along the Lagrangian trajectories and conditioned on the step-lengths d shows (Fig. 2(f)) that trajectories are less likely to have persistent, *directed* motion in regions of strong vorticity: Quiescent regions favour persistent motion (Fig. 1(b)).

While this is a useful starting point, it does not capture the two main geometrical effects—vortical and straining regions—which characterise (inertial and active) two-dimensional turbulence. A first approach to this problem is through the Okubo-Weiss parameter $\Lambda = (\omega^2 - \sigma^2)/4\langle \omega^2 \rangle$, where $\sigma^2 = S_{ij}S_{ij}$ is the square of the strain-rate $S_{ij} = (\nabla \mathbf{u} + \nabla \mathbf{u}^T)/2$, measured along individual trajectories: The sign of the Okubo-Weiss criterion [39, 40] determines if the particle is either in a vortical ($\Lambda > 0$) or a straining ($\Lambda < 0$) region as shown in Fig. 2(b) for the Eulerian vorticity field of panel (a).

Figure 2(g)—the Lagrangian pdf of Λ , measured along particle tracks and conditioned on step-lengths in a manner similar to panel (f)—while clearly showing an overall preferential bias for vortical regions, brings out the inference drawn before more clearly. Tracers are far more likely to move in long, straight segments when they are in regions of the flow where both ω and Λ have a small magnitude. This bias for persistent motion in quiescent regions of the flow is further affirmed by the joint distributions of tracer displacements d with ω and Λ as shown in Figs. 2(h) and 2(i), respectively. The insets in these panels are the same joint distributions but for $|\omega|$ and $|\Lambda|$. These clearly show that large displacements are more probable when both ω and Λ are small: Long straight excursions instead of diffusive meandering occur in these regions.

These distributions, however, cannot trace the *origins* of extremely coherent motion of tracers, illustrated in Fig. 1(b), which contribute most to the anomalous diffusive behaviour in highly active suspensions. This is because a simple decomposition of the flow field in terms of vortical and straining regions fails to capture a recently discovered [21] additional emergent *geometrical* feature (with no counterpart in inertial turbulence): *Streaks* which are striped structures with alternate signs of ω as seen in Fig. 2(a).

Are streaks the primary cause for persistent Lévy walks seen in our Lagrangian measurements? In fact, the local flow geometry, and how it evolves in time, essentially governs the fate of a trajectory that passes through it. We demonstrate this in Fig. 3, which shows representative close-by trajectories originating in (a) vortical, (b) streaky or (c) quiescent straining regions; the color panels above the trajectories show the vorticity in the small region of the flow where these trajectories originate. This immediately brings out the striking difference in the fate of tracers depending on where they are in the flow. While particles originating in vortical spots (Fig. 3(a)) travel diffusively and incoherently, the ones which start in streaky regions (Fig. 3(b)) form a coherent bundle with persistent and correlated motions. Trajectories originating in quiescent regions (Fig. 3(c)) show elements of both diffusive motion with periods of persistence.

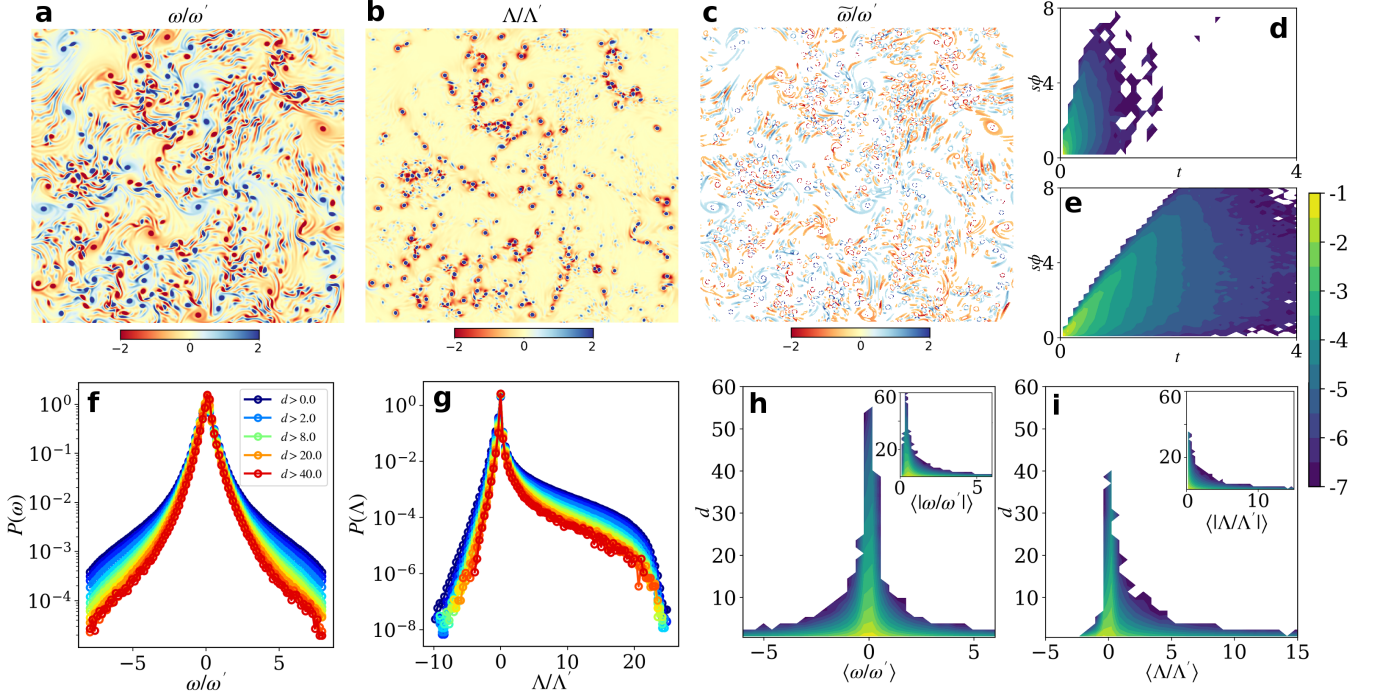


FIG. 2. Pseudocolor plots of the (a) vorticity ω , (b) Okubo-Weiss parameter Λ and (c) masked vorticity $\tilde{\omega}$ fields showing the vortical, straining and streaky patches. Joint-distributions of the residence time and normalised distances of particles (d) within and (e) outside the streaks showing streaks facilitating enhanced displacement in shorter times. Probability distribution functions of the Lagrangian history of (f) vorticity and (g) Okubo-Weiss criterion, conditionally sampled over trajectory segment lengths d , show that persistent segments pass preferentially through quiescent regions of ω and Λ . Joint distributions of the segment lengths d with (h) ω and (i) Λ (insets show the distribution with $|\omega|$ and $|\Lambda|$) further emphasise that the longer trajectory segments mostly occur in quiescent field regions (the colorbar for the joint distributions shows logarithmically spaced decades).

How, then, do we understand this puzzling behaviour? As the underlying field evolves, the trajectories which may have originated in a particular geometry of the flow are likely to encounter a different flow topology in time. This rules out mean-squared-displacements, conditioned on where trajectories originate, as a diagnostic for a couple of reasons. Firstly, such an exercise can be only performed up to short times during which the field remains largely unchanged. Secondly, these short-time time MSDs are invariably ballistic, regardless of where they originate. Hence, the subtle correlation between the emergent vagaries of the Eulerian field and the individual trajectories must be found within the Lagrangian history of particle dynamics.

But first, a sharper definition of what is a streak must be made which goes beyond the visual. To that end, careful measurements suggest that streaks coincide with places with (a) relatively moderate values of ω and (b) low magnitudes of Λ . This becomes clear upon comparing the vorticity field, in Fig. 2(a), with the Λ field at the same time instance, shown in Fig. 2(b). This hints at a criterion, albeit somewhat *ad-hoc*, for identifying the streak regions. We define streaks as regions of the flow where, locally, the vorticity is bounded from below and the Okubo-Weiss criterion is bounded from above, i.e., $\omega \geq \omega_T$ and $\Lambda \leq \Lambda_T$; we choose (and other similar choices give equally consistent results) thresholds $\omega_T = 0.5\omega'$ and $\Lambda_T = 0.1\Lambda'$. This criterion allows us to define a *mask* which, when applied to the vorticity field of active flows, generates a filtered field $\tilde{\omega} = \omega$ in streaks and 0 otherwise. In Fig. 2(c) we show $\tilde{\omega}$ for the same flow realisation as in panel (a) to demonstrate the accuracy of this criterion which goes beyond the binary classification of the Okubo-Weiss parameter and picks out the streaky regions.

With the definitions of the flow topologies in place, we can now unambiguously separate trajectories based on the flow regions they encounter. An obvious quantification is the joint distribution of tracer displacements s with residence times t in and out of streak regions. Since the streaky regions occupy a relatively small area-fraction A_f of the flow, it is useful to look at the effective displacements $\phi \equiv s/\sqrt{A_f}$ within a streak, and conversely $\phi \equiv s/(1 - \sqrt{A_f})$ outside it, to ascertain the relative degree to which streaky and non-streaky regions assist persistent motion.

While streaks form a small fraction ($\sim 12\%$) of the flow resulting in a relatively smaller residence time, tracers inside the (Fig. 2(d)) streaks are advected much farther within this short time than those outside (Fig. 2(e)). The joint

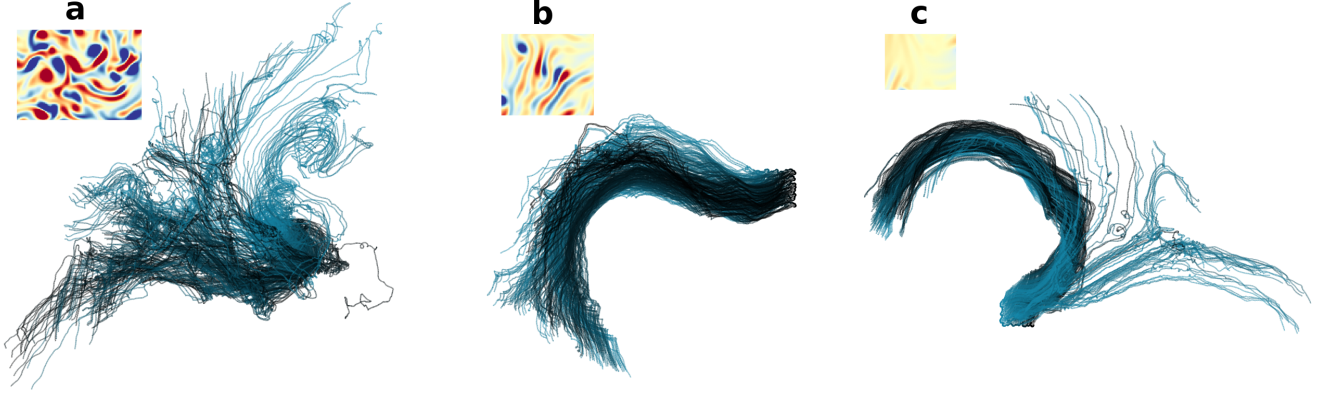


FIG. 3. Representative bundles of trajectories originating in (a) vortical spots, (b) streaks and (c) quiescent regions. While the trajectories spread incoherently in (a) and coherently in (b), there is a mix of both for (c). The trajectories are coloured, varying smoothly from blue (left edge) to black (right edge), based upon their x -coordinates with the colour and gives a sense of mixing vis-à-vis coherence in the trajectory bundles.

$\phi - t$ distribution is much wider when outside these special structures, indicating that large residence times (in purely vortical and straining patches) do not lead to large displacements. Thus, coherent, persistent motion is intrinsically correlated with the special flow patterns (Fig. 2(c)) that a bacterial suspension can spontaneously generate.

FIRST PASSAGE PROBLEM AND DYNAMICAL HETEROGENEITY

This surprising ability to exploit self-generated patterns and their emergent hydrodynamics to aid persistent motion accords individuals a distinct advantage to reach targets—for nutrition, for example—on much shorter time scales than it would be otherwise possible. While this was certainly implicit in earlier observations of anomalous diffusion through measurements of the mean-square-displacements [21], a direct way of looking at this is to ask how such activity-induced streaks enhance the efficacy of tracers in reaching distances R away. This, of course, is the much studied question in statistical physics of First Passage Problems [41–45], also used to quantify biological motility [46–48]: What is the statistics of the time t_R for tracers to reach (for the first time and be “absorbed” at) the boundary of a circle of radius R as illustrated in Fig. 1; see also <https://youtu.be/CPJ3Z1XBf-k>.

In the context of bacterial suspensions and living systems in general, the first passage characteristics are critical to how efficiently bacteria forage for food and survive. In an active turbulent flow, whose evolution is governed by Eq. (1), a bacterium foraging for food can be thought of as a point tracer being advected until it reaches the food source at a distance R , at which point the search is concluded.

The probability of a tracer reaching (and being absorbed by) a boundary R at time $t = t_R$ when it starts from $r = 0$ at $t = 0$ is given by the first passage probability distribution $P(R, t_R)$ which is calculated from the (survival) probability $S(t) = \int_0^R p(r, t) 2\pi r dr$ of not reaching the boundary in time t_R via $P(R, t_R) = -\frac{\partial S}{\partial t} \Big|_{t_R}$ [44, 49]. The survival probability assumes isotropy of the distribution $p(r, t)$ of tracers which, for low activities, satisfies the diffusion equation [50] with absorbing boundary condition $p(R, t) = 0$ and the initial condition $p(r, 0) = \delta(r)/2\pi r$. We begin by writing the Fokker-Planck equation in two-dimensions:

$$\partial_t p(r, t) = K_d \nabla^2 p(r, t) \quad (2)$$

K_d being the diffusion constant. Assuming a solution of the form $p(r, t) = u(r)f(t)$ yields separate differential equations for the temporal and radial parts to obtain:

$$u(r) = J_0(Cr) = \sum_{n=0}^{\infty} \frac{(-1)^n}{(n!)^2} \left(\frac{Cr}{2} \right)^{2n} \quad (3)$$

$$f(t) = f_0 e^{-C^2 K_d t} \quad (4)$$

where $f_0 = f(t)|_{t=0}$, and J_0 is the Bessel function of the first kind and order zero. By using the absorbing boundary condition to solve for the radial part $u(r)$, the delta-function initial condition to determine f_0 and the constraint that

$S(t=0) = 1$, we obtain

$$p(r, t) = \frac{1}{2\pi R^2 \left(\sum_i \frac{J_1(h_i)}{h_i} \right)} \sum_i J_0 \left(\frac{h_i r}{R} \right) e^{-h_i K_d t / R^2}; \quad (5)$$

thence the survival probability

$$S(t) = \int_0^R p(r, t) 2\pi r dr = \sum_i e^{-h_i K_d t / R^2} \frac{J_1(h_i)}{h_i}. \quad (6)$$

Here, J_1 is the Bessel function of the first kind and order one, whereas h_i are the zeros of $J_0(CR)$. The first passage time distribution is then simply

$$P(R, t_R) = -\partial_t S|_{t=t_R} = \frac{K_d}{R^2} \sum_i e^{-h_i K_d t_R / R^2} J_1(h_i) \quad (7)$$

The dominant contribution to the first passage distribution comes from the smallest $h_i = A$ and yields the well-known result: $P(R, t_R) \sim \frac{K_d}{R^2} e^{-AK_d t_R / R^2}$ [51]. The first passage distribution can be generalised to the case of anomalous diffusion as $P(R, t_R) \sim e^{-t_R / R^{2/\xi}}$, where the scaling exponent $1 \leq \xi \leq 2$ is a consequence of the anomalous diffusion in the mean-square-displacement $\Delta x^2 \sim t^\xi$ (and which can also be obtained analytically by solving the fractional Fokker-Planck equation [49, 52–55]).

In the inset of Fig. 4(a) we show the first passage time distributions for different values of R which collapse on to a unique curve when the first passage times are scaled as t_R / R^2 (Fig. 4(a)) consistent with our theoretical prediction for moderately active suspensions. On making suspensions more active, as shown in Fig. 4(b), the diffusive t_R / R^2 scaling still remains approximately true but only for large values of R . Indeed, for smaller values of R (Fig. 4(b), inset), the distributions collapse only when the first passage times are scaled as $t_R / R^{3/2}$, accounting for the enhanced motility. This is because at such short distances, persistent trajectories contribute to the statistics of first passage overwhelmingly and hence the scaling exponent associated with anomalous diffusion in such systems, $\xi \approx 4/3$ [21], leads to an anomalous form of the first passage distribution.

While the normalized first passage distributions give a statistical sense for an *ensemble* of trajectories, it does not allow us to have a sense of the variations, within an ensemble, of individual trajectories. Since tracers sample the entire phase space, the issue of an incipient *dynamical heterogeneity* in the flow is a vexing one.

In order to understand this, we take a fraction (10%, for sufficient statistics) of the fastest and slowest trajectories that reach various target radii R , for different values of α . Visually, the fastest and slowest trajectories are different: The former mostly straight and persistent, while the latter convoluted and meandering for *all* levels of activity. However, the Lagrangian history of these tracers, i.e., the Λ values they encounter before hitting their targets, shows, as illustrated in the inset of Fig. 4(c) that at mild levels of activity there is no distinction between the underlying Eulerian field sampled by the fastest and slowest tracers. These conditional distributions of the Okubo-Weiss parameter show that the heterogeneity in trajectories, up to intermediate levels of activity, is simply a statistical consequence of the *random* sampling of the flow. However, for highly active suspension, where anomalous diffusion becomes robust, signatures of dynamical heterogeneity, as seen in the clearly different Lagrangian histories of the fastest and slowest trajectories (see Fig. 4(c), manifest themselves. Consistent with the findings so far that persistent motion favours quiescent field regions, the fastest tracers sample milder regions of the Okubo-Weiss field, in comparison to the slowest tracers. This distinction, moreover, is starker for smaller R values, while at large values of R , the tracers begin to experience (statistically) similar underlying fields.

This evidence for dynamical heterogeneity in the flow, such that the variation in the nature of trajectories is not *merely* statistical as happens in inertial turbulence [56], is further strengthened by looking at where in the flow do the fastest and slowest tracers originate, for a given value of R . In other words, do trajectories get *lucky* by being at the right place at the right time, which allows them to reach their targets faster than others? This would suggest that for highly active suspensions, the initial locations of these fast, lucky trajectories must be clustered in nearby regions while for less active flows they are more uniformly distributed. In the inset of Fig. 4(d), we show a plot of the starting points of the fastest 1% of the trajectories for a target at $R = 15$. We indeed find that for the highly active suspensions ($\alpha = -6$) these points remain strongly clustered, unlike the random and uniform distribution seen for the less active ($\alpha = -1$) case. While confirming a dynamically heterogeneous flow, this also explains the bundling of these trajectories already seen in Fig. 1(b), where the fastest tracers (after their initial locations are artificially superimposed at the center of the circle), evolve as coherent *bundles*, arriving at their target circle and forming a very anisotropic distribution around the circumference. This is because the bundles originate clustered together in a few special locations in the flow and hence follow very similar trajectories. We quantify the degree of this clustering by

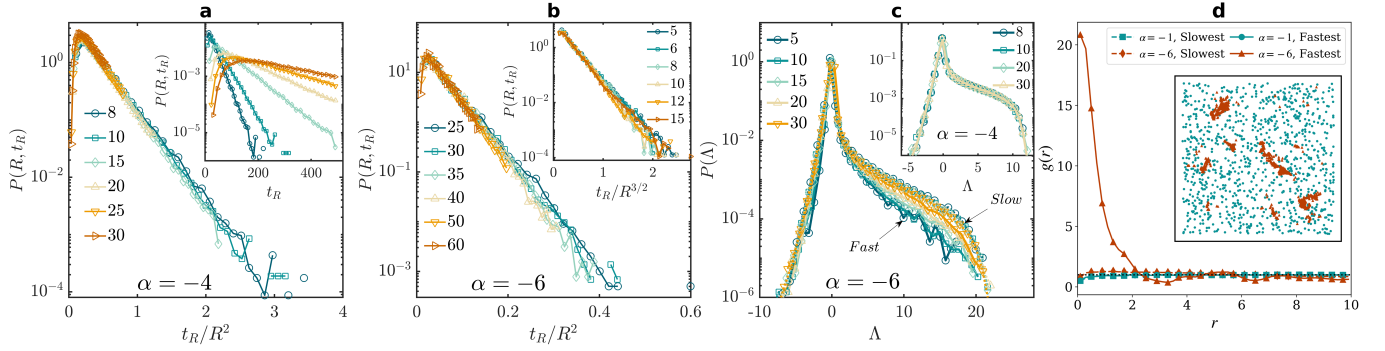


FIG. 4. (a) Semi-log plots of the first passage distributions for mildly active suspensions collapse on a single curve for rescaled time t_R/R^2 corresponding the diffusive transport for different values of R ; the inset shows the same without the rescaling of time. (b) Analogous plots for highly active suspensions show a similar diffusion-driven collapse *only* for large distances and time; for short distance (inset) the curves collapse when time is rescaled as $t_R/R^{3/2}$ which factors in anomalous diffusion. (c) Probability distribution functions of Λ conditioned on the fastest (solid-lines) and slowest (dashed-lines) 10% of tracers for $\alpha = -6$ and $\alpha = -4$ (inset) and for various target radii R . The distributions differ only for the highly active suspension and for small R showing the emergence of a true dynamical heterogeneity. This is visually illustrated in the inset of panel (d) showing that the origins of the fastest 1% tracers for $\alpha = -1$ are randomly distributed whereas those for $\alpha = -6$ are strongly localised suggesting “lucky” spots for efficient motility. This is confirmed in (d) measurements of the pair-distribution function which gives a pronounced peak for the fastest tracer origins for $\alpha = -6$, while rapidly converging to the uniform distribution $g(r) = 1$. Similar measurements for the fastest tracers for lower activity and indeed for the slowest trajectories for all activity show uniform distribution throughout.

calculating the pair-distribution function $g(r)$, for the fastest and slowest 1% of the tracers, in Fig. 4(d). The $g(r)$ of the origins of the slowest tracers quickly attains a value close to 1, irrespective of activity, corresponding to a uniform (or ideal-gas) distribution of points (albeit with a small overshoot for $\alpha = -6$ at small r , showing weak preferential clustering also for the slowest tracers). The fastest tracer origins for high activity show a pronounced peak in the pair distribution at small values of r , reflecting the presence of these lucky spots. At mild activity, the $g(r)$ for the fastest tracer origins rapidly attains to a value of 1 as well, reflecting the fact that the heterogeneity of trajectories is merely statistical.

PAIR-DISPERSION

So far we have focussed our attention on single-particle statistics. But before we conclude, we must consider the implications of these anomalies on the Richardson-Obukhov pair-dispersion problem [57, 58] which informs much of our understanding of inertial turbulence [59]. Pair-dispersion is simply the statistics of separation of particle pairs that originate within a small distance ϵ of each other measured as $\langle r_p^2(t) \rangle = \langle |\mathbf{x}_1(t) - \mathbf{x}_2(t)|^2 \rangle$, where $\mathbf{x}_1(t)$ and $\mathbf{x}_2(t)$ are the positions of a particle pair, with $|\mathbf{x}_1(0) - \mathbf{x}_2(0)| = \epsilon$ being their initial separation, and $\langle \cdot \rangle$ denotes averaging over all particle pairs.

Figure 5(a) shows pair-separation for increasingly active suspensions, with $\epsilon = 0.001$. Interestingly, the influence of activity appears to be mild, with only a slight change in the extent of the intermediate scaling; even for $\alpha = -6$, a scaling regime seems to extend only up to a decade. The limited extent of scaling, and its significant deviation from the Richardson prediction $\sim t^3$ for inertial turbulence, may stem from the lack of an inertial range in active turbulence. It has been shown that active turbulence, at least using the nematohydrodynamic model and other minimal models for wet active nematics [4, 60, 61], does not have an energy cascade resulting from non-linear mode interactions. While, admittedly, our model differs from these, it is likely that a similar situation arises here. In fact, the presence of a particularly wide inertial range and scale separation (effectively, a large Reynolds number) is essential to observe the Richardson scaling regime even in inertial turbulence, despite cascade dynamics, and persistent motion in trajectories (ballistic Lévy walks) can further lead to deviation from Richardson scaling [62]. While there is no natural way to increase scale separation in our system, we tested various domain sizes for $\alpha = -6$, from $L = 20$ (on $N = 1024$) to $L = 80$ (on $N = 4096$), and obtained identical pair-separation curves, without an increase in the extent of scaling. The inset of Fig. 5(a) shows the influence of the initial separation ϵ on pair-separation for $\alpha = -6$. As ϵ decreases, the slope of the intermediate range increases significantly. This ϵ dependence is consistent with findings from two-dimensional inertial turbulence [63, 64], and the apparent steepening of the slope is a consequence of an exponential

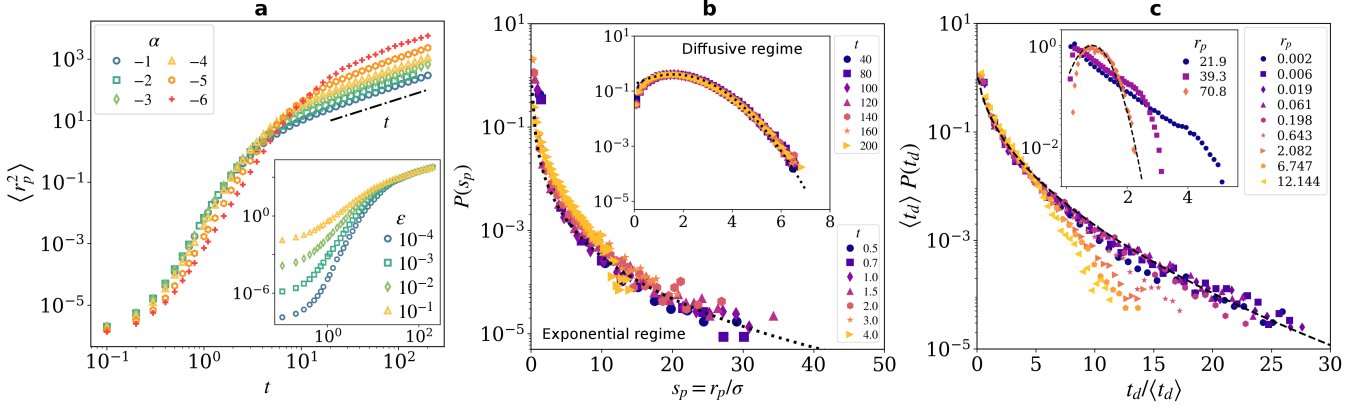


FIG. 5. (a) The dependence of the relative pair separation on α (with $\epsilon = 0.001$) and (inset) on ϵ (for $\alpha = -6$). (b) Probability distribution of the normalized pair separation s_p follows a stretched exponential for times up to diffusive pair-separation, whence (inset) the distribution becomes Gaussian. (c) The probability distribution of pair-separation doubling times t_d are also stretched exponentials at small separations; the curves become steeper with increasing r_p and (inset) converge to a Gaussian distribution for large r_p .

initial separation tending to diffusive separation at longer times.

In the absence of robust Richardson scaling, other pair-separation measures have been proposed to quantify dispersion statistics [62, 65]. One such is the probability distribution of pair-separations r_p , at different times during the growth of $\langle r_p^2 \rangle$. Figure 5(b) shows the probability distribution of the rescaled (with the variance) pair-separations $s_p = r_p/\sigma$, at various time instances, for trajectories with an initial separation of $\epsilon = 0.001$ and for $\alpha = -6$. The separations s_p collapse to a single stretched-exponential distribution while at very long times, well into the diffusive pair-separation regime $\langle r_p^2 \rangle \sim t$, the s_p distribution becomes Gaussian. All this is consistent with findings from two-dimensional inertial turbulence [63, 65], where a stretched-exponential and Gaussian distribution of rescaled separations is found for the forward enstrophy-cascade and inverse energy-cascade regimes, respectively. This shows that the pair-separation process is self-similar in time, following different distributions during the rapid and (eventually) diffusive growth.

Related to the first passage problem, we consider the distribution of separation doubling-times [62, 63]. This is defined as the time t_d it takes for an initial separation r_p to grow to a scale ρr_p . Here, we can also expect an influence of the persistence in trajectories. Smaller initial separations r_p will lead to longer correlated motion, as trajectory-pairs will sample similar flow geometries (Fig. 3). This would lead to relatively longer doubling times, and a wider t_d distribution. At large initial separations, where trajectory-pairs are essentially uncorrelated to begin with, the separation doubling will occur more rapidly. This is precisely what is observed in Fig. 5(c) for $\rho = 1.8$; our results are similar for other ρ values that are not too small. The distributions of doubling-times t_d , normalized by the mean doubling time $\langle t_d \rangle$, for small values of r_p , follow a stretched exponential function, similar to two-dimensional inertial turbulence in the enstrophy-cascade range [63]. The distributions become steeper with increasing r_p , reflecting the decorrelation within trajectory pairs. The inset of Fig. 5(c) shows that at very large values of r_p , deep into the diffusive pair-separation phase, the distribution of t_d , as anticipated, approaches a Gaussian.

CONCLUSIONS

Anomalous diffusion and Lévy walks are common place in a wide variety of biological systems. However, in dense suspensions of microorganisms, such as bacterial swarms, which are a typical example of flowing active matter and a testing ground for active turbulence, the experimental evidence for such phenomena is only recent [20]. Furthermore, theoretical studies have been unable to go beyond the simple diffusion picture and predict, detect or understand the emergence of such super-diffusive regimes in active turbulence. This issue was resolved by a recent work [21] showing that anomalous Lagrangian statistics manifest only in extremely active suspensions, with $\alpha \sim -6$. Further exploring such highly active suspensions consistently revealed signatures of anomalies in Lagrangian measurements. The streaky flow regions, together with an emergent dynamical heterogeneity, contrive to selectively propel tracers persistently and aid in anomalous first-passage statistics. The results presented in this work should be readily amenable to experimental measurements in super-diffusive bacterial swarms, as well as in a diverse class of active flows. Whether the conjoined emergence of Eulerian streaks at high activity, and their role in promoting persistent motion, is universal, remains

to be ascertained, and the true mechanisms for manifesting Lagrangian anomalies may well be system dependent. Notwithstanding, we feel that our results show a biologically crucial aspect of the generalized hydrodynamics model beyond what has been previously observed, extending its applicability to a realm closer to experimental observations.

Further, measures like pair-dispersion mirror fundamental quantities like Lyapunov exponents, that characterize chaos in both diverging trajectories and solutions of the hydrodynamic equations. For instance, the flow Lyapunov exponent is known to increase with Reynolds number in inertial turbulence approximately as $\sim \text{Re}^{1/2}$ [66–68]. The analogous effect of activity on Lyapunov exponents in active turbulence remains unknown and is part of ongoing work, both within the Eulerian [66–68] and Lagrangian framework [69, 70], which looks at different aspects of many-body chaos [71] in such systems. Indeed, a complete understanding of the dynamical facets of active turbulence calls for a complete characterization of the skeleton of chaos underlying active flows. It is interesting to note that a recent work [72] on the (Lagrangian) irreversibility in such suspensions shows similar anomalies between active and inertial turbulence. Lastly, our work also lays out a systematic framework for the Lagrangian analysis of active flows, including measures for identifying geometrical structures emerging in the Eulerian fields. Adopting these in future work will not only ascertain the extent of universality of active turbulence anomalies, but also help connect hydrodynamic theories of active matter more closely to the physical picture.

ACKNOWLEDGMENTS

We thank Martin James for several useful discussions. The simulations were performed on the ICTS clusters *Tetris*, and *Contra*. SSR acknowledges SERB-DST (India) project DST (India) project MTR/2019/001553 and STR/2021/000023 for financial support. The authors acknowledge the support of the DAE, Govt. of India, under project no. 12-R&D-TFR-5.10-1100 and project no. RTI4001

-
- [1] M. C. Marchetti, J. F. Joanny, S. Ramaswamy, T. B. Liverpool, J. Prost, Madan Rao, and R. Aditi Simha, “Hydrodynamics of soft active matter,” *Rev. Mod. Phys.* **85**, 1143–1189 (2013).
 - [2] Sriram Ramaswamy, “Active matter,” *Journal of Statistical Mechanics: Theory and Experiment* **2017**, 054002 (2017).
 - [3] Amin Doostmohammadi, Jordi Ignés-Mullol, Julia M Yeomans, and Francesc Sagués, “Active nematics,” *Nature communications* **9**, 1–13 (2018).
 - [4] Ricard Alert, Jaume Casademunt, and Jean-Francois Joanny, “Active turbulence,” *Annual Review of Condensed Matter Physics* **13**, null (2022), <https://doi.org/10.1146/annurev-conmatphys-082321-035957>.
 - [5] John Toner, Yuhai Tu, and Sriram Ramaswamy, “Hydrodynamics and phases of flocks,” *Annals of Physics* **318**, 170–244 (2005), special Issue.
 - [6] Julia M. Yeomans, “Playful topology,” *Nature Materials* **13**, 1004–1005 (2014).
 - [7] Henricus H. Wensink, Jörn Dunkel, Sebastian Heidenreich, Knut Drescher, Raymond E. Goldstein, Hartmut Löwen, and Julia M. Yeomans, “Meso-scale turbulence in living fluids,” *Proceedings of the National Academy of Sciences* **109**, 14308–14313 (2012).
 - [8] Jörn Dunkel, Sebastian Heidenreich, Knut Drescher, Henricus H. Wensink, Markus Bär, and Raymond E. Goldstein, “Fluid dynamics of bacterial turbulence,” *Phys. Rev. Lett.* **110**, 228102 (2013).
 - [9] Kun-Ta Wu, Jean Bernard Hishamunda, Daniel TN Chen, Stephen J DeCamp, Ya-Wen Chang, Alberto Fernández-Nieves, Seth Fraden, and Zvonimir Dogic, “Transition from turbulent to coherent flows in confined three-dimensional active fluids,” *Science* **355** (2017), [10.1126/science.aal1979](https://doi.org/10.1126/science.aal1979).
 - [10] Tim Sanchez, Daniel T. N. Chen, Stephen J. DeCamp, Michael Heymann, and Zvonimir Dogic, “Spontaneous motion in hierarchically assembled active matter,” *Nature* **491**, 431–434 (2012).
 - [11] Yutaka Sumino, Ken H. Nagai, Yuji Shitaka, Dan Tanaka, Kenichi Yoshikawa, Hugues Chaté, and Kazuhiro Oiwa, “Large-scale vortex lattice emerging from collectively moving microtubules,” *Nature* **483**, 448–452 (2012).
 - [12] Yael Katz, Kolbjørn Tunstrøm, Christos C. Ioannou, Cristián Huepe, and Iain D. Couzin, “Inferring the structure and dynamics of interactions in schooling fish,” *Proceedings of the National Academy of Sciences* **108**, 18720–18725 (2011).
 - [13] Sriram Ramaswamy, “The mechanics and statistics of active matter,” *Annual Review of Condensed Matter Physics* **1**, 323–345 (2010).
 - [14] Andrea Cavagna, Alessio Cimarelli, Irene Giardina, Giorgio Parisi, Raffaele Santagati, Fabio Stefanini, and Massimiliano Viale, “Scale-free correlations in starling flocks,” *Proceedings of the National Academy of Sciences* **107**, 11865–11870 (2010).
 - [15] L Giomi, L Mahadevan, B Chakraborty, and M F Hagan, “Banding, excitability and chaos in active nematic suspensions,” *Nonlinearity* **25**, 2245–2269 (2012).
 - [16] Ricard Alert, Jean-François Joanny, and Jaume Casademunt, “Universal scaling of active nematic turbulence,” *Nature Physics* **16**, 682–688 (2020).

- [17] Xiao-Lun Wu and Albert Libchaber, “Particle diffusion in a quasi-two-dimensional bacterial bath,” *Physical review letters* **84**, 3017 (2000).
- [18] Hüseyin Kurtuldu, Jeffrey S Guasto, Karl A Johnson, and Jerry P Gollub, “Enhancement of biomixing by swimming algal cells in two-dimensional films,” *Proceedings of the National Academy of Sciences* **108**, 10391–10395 (2011).
- [19] Alexander Morozov and Davide Marenduzzo, “Enhanced diffusion of tracer particles in dilute bacterial suspensions,” *Soft Matter* **10**, 2748–2758 (2014).
- [20] Gil Ariel, Amit Rabani, Sivan Benisty, Jonathan D Partridge, Rasika M Harshey, and Avraham Be’Er, “Swarming bacteria migrate by lévy walk,” *Nature communications* **6**, 1–6 (2015).
- [21] Siddhartha Mukherjee, Rahul K. Singh, Martin James, and Samriddhi Sankar Ray, “Anomalous diffusion and lévy walks distinguish active from inertial turbulence,” *Phys. Rev. Lett.* **127**, 118001 (2021).
- [22] Sanjay C.P. and Ashwin Joy, “Friction scaling laws for transport in active turbulence,” *Physical Review Fluids* **5**, 024302 (2020).
- [23] M. F. Shlesinger, B. J. West, and J. Klafter, “Lévy dynamics of enhanced diffusion: Application to turbulence,” *Phys. Rev. Lett.* **58**, 1100–1103 (1987).
- [24] P. Dhar, Th. M. Fischer, Y. Wang, T. E. Mallouk, W. F. Paxton, and A. Sen, “Autonomously moving nanorods at a viscous interface,” *Nano Letters* **6**, 66–72 (2006).
- [25] Oleg V. Bychuk and Ben O’Shaughnessy, “Anomalous surface diffusion: A numerical study,” *The Journal of Chemical Physics* **101**, 772–780 (1994).
- [26] Matthew F. Krummel, Frederic Bartumeus, and Audrey Gérard, “T cell migration, search strategies and mechanisms,” *Nature Reviews Immunology* **16**, 193–201 (2016).
- [27] Blaine J. Cole, “Fractal time in animal behaviour: the movement activity of drosophila,” *Animal Behaviour* **50**, 1317–1324 (1995).
- [28] Florian Zanger, Hartmut Löwen, and Jürgen Saal, “Analysis of a living fluid continuum model,” in *Mathematics for Nonlinear Phenomena: Analysis and Computation: International Conference in Honor of Professor Yoshikazu Giga on his 60th Birthday* (Springer, 2015) pp. 285–303.
- [29] Ju Swift and Pierre C Hohenberg, “Hydrodynamic fluctuations at the convective instability,” *Physical Review A* **15**, 319 (1977).
- [30] John Toner and Yuhai Tu, “Long-range order in a two-dimensional dynamical XY model: How birds fly together,” *Phys. Rev. Lett.* **75**, 4326–4329 (1995).
- [31] John Toner and Yuhai Tu, “Flocks, herds, and schools: A quantitative theory of flocking,” *Phys. Rev. E* **58**, 4828–4858 (1998).
- [32] Martin James and Michael Wilczek, “Vortex dynamics and lagrangian statistics in a model for active turbulence,” *The European Physical Journal E* **41**, 21– (2018).
- [33] Sanjay C. P. and Ashwin Joy, “Friction scaling laws for transport in active turbulence,” *Phys. Rev. Fluids* **5**, 024302 (2020).
- [34] Martin James, Dominik Anton Suchla, Jörn Dunkel, and Michael Wilczek, “Emergence and melting of active vortex crystals,” *Nature Communications* **12**, 5630 (2021).
- [35] Imre M Jánosi, John O Kessler, and Viktor K Horváth, “Onset of bioconvection in suspensions of bacillus subtilis,” *Physical Review E* **58**, 4793 (1998).
- [36] Andrey Sokolov and Igor S Aranson, “Physical properties of collective motion in suspensions of bacteria,” *Physical review letters* **109**, 248109 (2012).
- [37] Casey Reas and Ben Fry, *Processing: a programming handbook for visual designers and artists* (Mit Press, 2007).
- [38] Matt Pearson, *Generative art: a practical guide using Processing* (Simon and Schuster, 2011).
- [39] Akira Okubo, “Horizontal dispersion of floatable particles in the vicinity of velocity singularities such as convergences,” *Deep Sea Research and Oceanographic Abstracts* **17**, 445–454 (1970).
- [40] John Weiss, “The dynamics of enstrophy transfer in two-dimensional hydrodynamics,” *Physica D: Nonlinear Phenomena* **48**, 273–294 (1991).
- [41] S. Chandrasekhar, “Stochastic problems in physics and astronomy,” *Rev. Mod. Phys.* **15**, 1–89 (1943).
- [42] Alan J. Bray, Satya N. Majumdar, and Grégory Schehr, “Persistence and first-passage properties in nonequilibrium systems,” *Advances in Physics* **62**, 225–361 (2013).
- [43] Sidney Redner, *A Guide to First-Passage Processes* (Cambridge University Press, 2001).
- [44] Venkataraman Balakrishnan, *Elements of nonequilibrium statistical mechanics* (Springer, 2021).
- [45] Ralf Metzler, Sidney Redner, and Gleb Oshanin, *First-passage phenomena and their applications*, Vol. 35 (World Scientific, 2014).
- [46] Tom Chou and Maria R D’Orsogna, “First passage problems in biology,” in *First-passage phenomena and their applications* (World Scientific, 2014) pp. 306–345.
- [47] Konark Bisht, Stefan Klumpp, Varsha Banerjee, and Rahul Marathe, “Twitching motility of bacteria with type-iv pili: Fractal walks, first passage time, and their consequences on microcolonies,” *Phys. Rev. E* **96**, 052411 (2017).
- [48] Hamid Teimouri and Anatoly B. Kolomeisky, “Theoretical investigation of stochastic clearance of bacteria: first-passage analysis,” *Journal of The Royal Society Interface* **16**, 20180765 (2019).
- [49] Arnold J. F. Siegert, “On the first passage time probability problem,” *Phys. Rev.* **81**, 617–623 (1951).
- [50] Hannes Risken and Till Frank, *The Fokker-Planck Equation* (Springer, 1996).
- [51] Akhilesh Kumar Verma, Akshay Bhatnagar, Dhruvadya Mitra, and Rahul Pandit, “First-passage-time problem for tracers in turbulent flows applied to virus spreading,” *Phys. Rev. Research* **2**, 033239 (2020).
- [52] Govindan Rangarajan and Mingzhou Ding, “First passage time distribution for anomalous diffusion,” *Physics Letters A*

- 273**, 322–330 (2000).
- [53] Govindan Rangarajan and Mingzhou Ding, “Anomalous diffusion and the first passage time problem,” *Phys. Rev. E* **62**, 120–133 (2000).
 - [54] M. Gitterman, “Mean first passage time for anomalous diffusion,” *Phys. Rev. E* **62**, 6065–6070 (2000).
 - [55] Vladimir V Palyulin, George Blackburn, Michael A Lomholt, Nicholas W Watkins, Ralf Metzler, Rainer Klages, and Aleksei V Chechkin, “First passage and first hitting times of lévy flights and lévy walks,” *New Journal of Physics* **21**, 103028 (2019).
 - [56] R Scatamacchia, L Biferale, and F Toschi, “Extreme events in the dispersions of two neighboring particles under the influence of fluid turbulence,” *Physical review letters* **109**, 144501 (2012).
 - [57] Lewis Fry Richardson and Gilbert Thomas Walker, “Atmospheric diffusion shown on a distance-neighbour graph,” *Proceedings of the Royal Society of London. Series A, Containing Papers of a Mathematical and Physical Character* **110**, 709–737 (1926).
 - [58] AM Obukhov, “On the distribution of energy in the spectrum of turbulent flow,” *Bull. Acad. Sci. USSR, Geog. Geophys.* **5**, 453–466 (1941).
 - [59] Juan PLC Salazar and Lance R Collins, “Two-particle dispersion in isotropic turbulent flows,” *Annual review of fluid mechanics* **41**, 405–432 (2009).
 - [60] J. Urzay, A. Doostmohammadi, and J. M. Yeomans, “Multi-scale statistics of turbulence motorized by active matter,” *Journal of Fluid Mechanics* **822**, 762–773 (2017).
 - [61] L. N. Carenza, L. Biferale, and G. Gonnella, “Cascade or not cascade? energy transfer and elastic effects in active nematics,” *EPL (Europhysics Letters)* **132**, 44003 (2020).
 - [62] G. Boffetta and I. M. Sokolov, “Statistics of two-particle dispersion in two-dimensional turbulence,” *Physics of Fluids* **14**, 3224–3232 (2002).
 - [63] M. K. Rivera and R. E. Ecke, “Pair dispersion and doubling time statistics in two-dimensional turbulence,” *Phys. Rev. Lett.* **95**, 194503 (2005).
 - [64] H. Xia, N. Francois, B. Faber, H. Punzmann, and M. Shats, “Local anisotropy of laboratory two-dimensional turbulence affects pair dispersion,” *Physics of Fluids* **31**, 025111 (2019).
 - [65] Marie-Caroline Jullien, Jérôme Paret, and Patrick Tabeling, “Richardson pair dispersion in two-dimensional turbulence,” *Phys. Rev. Lett.* **82**, 2872–2875 (1999).
 - [66] Siddhartha Mukherjee, Jérôme Schalkwijk, and Harmen J. J. Jonker, “Predictability of dry convective boundary layers: An les study,” *Journal of the Atmospheric Sciences* **73**, 2715 – 2727 (2016).
 - [67] G. Boffetta and S. Musacchio, “Chaos and predictability of homogeneous-isotropic turbulence,” *Phys. Rev. Lett.* **119**, 054102 (2017).
 - [68] Arjun Berera and Richard D. J. G. Ho, “Chaotic properties of a turbulent isotropic fluid,” *Phys. Rev. Lett.* **120**, 024101 (2018).
 - [69] Jeremie Bec, Luca Biferale, Guido Boffetta, Massimo Cencini, Stefano Musacchio, and Federico Toschi, “Lyapunov exponents of heavy particles in turbulence,” *Physics of Fluids* **18**, 091702 (2006).
 - [70] Samriddhi Sankar Ray, “Non-intermittent turbulence: Lagrangian chaos and irreversibility,” *Phys. Rev. Fluids* **3**, 072601 (2018).
 - [71] Suga D. Murugan, Dheeraj Kumar, Subhro Bhattacharjee, and Samriddhi Sankar Ray, “Many-body chaos in thermalized fluids,” *Phys. Rev. Lett.* **127**, 124501 (2021).
 - [72] Kolluru Venkata Kiran, Anupam Gupta, Akhilesh Kumar Verma, and Rahul Pandit, “Irreversibility in bacterial turbulence: Insights from the mean-bacterial-velocity model,” arXiv:2201.12722 (2022).